MAGNETIC RESONANCE IN MEDICINE 26, 16–39 (1992)

Theory of Contrast Agents in Magnetic Resonance Imaging: Coupling of Spin Relaxation and Transport

W. R. BAUER* AND K. SCHULTEN

Beckman Institute and Department of Physics, University of Illinois, 405 North Mathews Street, Urbana, Illinois 61801

Received May 3, 1990; revised July 22, 1991; accepted August 8, 1991

The role of diffusive transport on the enhancement of nuclear spin relaxation through NMR contrast agents is described by means of diffusion-Bloch equations. These equations are solved in the mean relaxation time approximation [W. Nadler and K. Schulten, *J. Chem. Phys.* **82,** 151–160 (1985)]. A model presented considers relaxation enhancement in tissue in which contrast agents confined to intravascular spaces affect nuclear spin in the extravascular volume. We show how the mean relaxation time depends on capillary density, on permeability, and on diffusion. A second model describes enhanced phase relaxation of liver tissue in the presence of magnetic particles in Kupffer cells. The relationship between relaxation rate and density of Kupffer cells is investigated. The diagnostic value of enhanced nuclear relaxation in the presence of contrast agents is discussed on the basis of the systematic mathematical results obtained.

1. INTRODUCTION

Contrast in magnetic resonance imaging (MRI) originates from the signal intensity of tissue and is due to magnetization of the nuclear spins detected by the instrument, usually protons. The nuclear magnetization is determined by the pulse sequence applied in the NMR imaging procedure, by the density of the nuclear spin subfractions, e.g., water protons or protons of fats, and by the spin–lattice relaxation time T_1 and phase relaxation time T_2 of each nuclear spin subfraction.

The concentration of nuclear spin subfractions and the respective relaxation times depend on tissue type. Tissues which differ in nuclear spin subfraction composition and in relaxation times produce different total nuclear magnetizations and, hence, can be distinguished by different signal intensities in MRI. On the other hand, tissues with identical nuclear spin subfraction compositions and relaxation times cannot be distinguished.

An approach to contrast enhancement and contrast differences is furnished by NMR contrast agents, substances which shorten to various degrees spin–lattice and/or phase relaxation times and, thus, alter the signal intensity of tissues. This enables one to distinguish regions of tissue with different concentration or with different activities of contrast agent.

An effect of transport on the activity of NMR contrast agents in tissues can develop as follows. Due to their pharmacological properties contrast agents can exhibit a specific

* Present address: Medical School, University of Würzburg, Würzburg, Germany.

0740-3194/92 $5.00

distribution in tissue, e.g., they may be located in the intravascular space (*1*) or in special macrophages of liver tissue (*2*). Contrast agents, if confined to specific compartments in tissue, may develop their contrast enhancement effect mainly through transport across compartmental boundaries and intracompartmental diffusion. In this paper we will explain this possibility in terms of two mathematical models.

The models presented in this paper describe two different types of contrast agents, (i) intravascular contrast agents and (ii) superparamagnetic or ferromagnetic particles in macrophages (Kupffer cells) of liver. The models are based on spatially inhomogeneous relaxation of nuclear magnetization. The overall relaxation behavior for such model systems will be calculated as a function of inhomogeneous diffusion parameters in tissue. We will show that diffusive transport of water is most likely the relevant mechanism for enhancement of nuclear magnetization relaxation in tissue by several common NMR contrast agents. Since pathological processes may affect transport parameters, we will then outline how such conditions could alter relaxation times of nuclear magnetization.

Our models for the effect of NMR contrast agents in tissue describe generic types of relaxation inhomogenities in tissue. Beyond the examples discussed below the description developed in the present paper can be applied to liposome systems as carriers for contrast agents (*3, 4*), to spleen, bone marrow, and cell suspensions as model systems. The nature of the mathematical treatment used for the modeling, i.e., diffusion-Bloch equations, limits our descriptions to ideal circumstances. More realistic situations need to be modeled by computer simulations. The theory presented below can guide such simulations as well as provide valuable tests for such simulations.

2. MECHANISM OF ACTION OF VASCULAR NMR CONTRAST AGENTS

2.1. Review of NMR Contrast Agents

Vascular NMR contrast agents are substances which are injected into blood vessels and which enhance relaxation and, thereby, affect the contrast in NMR images of tissue supported by blood vessels. The contrast enhancement efficiency is determined by the local density of blood vessels. Substances used as contrast agents are paramagnetic lanthanide ion chelates like Gd-DTPA and Dy-DTPA (DTPA = diethylenetriamine pentaacetate) (*5*) and lanthanide chelates linked to macromolecules like albumin-$(Gd\text{-}DTPA)_{18}$ (*1*).

In this section we will only consider situations in which agents develop their contrast enhancing effect while remaining in the intravascular space. Such agents are the lanthanide chelates linked to macromolecules, e.g., albumin-$(Gd\text{-}DTPA)_{18}$, which, except in liver, spleen, and bone marrow, stay within the intravascular space; furthermore, the agents Gd-DTPA and Dy-DTPA in brain belong to the group considered as it is known that these agents remain within the intravascular space (blood–brain barrier) (*5*). The mentioned agents have been observed to reduce the nuclear spin relaxation time. Schmiedl *et al.* observed that albumin-$(Gd\text{-}DTPA)_{18}$ in heart tissue decreases the spin–lattice relaxation time (T_1) from about 520 ms to 300 ms (*1*). Villringer *et al.* observed a 50% reduction of phase relaxation times (T_2) in brain (*5*). Due to the short range of dipole–dipole interaction (*6*) these contrast agents interact directly with intravascular nuclear spins only. However, the following consideration will show that

intravascular contrast agents bring about a relaxation of extravascular nuclear magnetization.

The fraction of the intravascular space in heart, for example, is about 7% of total volume (*7*), and as the concentration of water molecules is about the same in intra- and extravascular space (*8*), the intravascular water proton fraction is also less than 7% of total proton number. If one assumes that the observed effect of the agent is limited only to the intravascular proton fraction of 7%, intra- and extravascular nuclear magnetization would relax independently. The overall relaxation time T of two independent fractions of tissue is derived from a magnetization decay $M(t) = f_{iv}\exp(-t/T_{iv}) + f_{ev}\exp(-t/T_{ev})$, where f_{iv}, f_{ev} is the fraction of intravascular/extravascular protons with the corresponding relaxation time T_{iv}, T_{ev}.[1] Assuming a single exponential decay, $M(t) = \exp(-t/T)$ one derives for the overall relaxation time, $T = \int_0^\infty dtM(t) = f_{iv}T_{iv} + f_{ev}T_{ev}$.

We want to apply this formula to an observation of spin–lattice relaxation times T_1. Assuming a relaxation time of proton spins in blood with albumin-(Gd-DTPA)$_{18}$ of 88 ms (*1*) and a relaxation time of heart tissue of 500 ms (this value has been adjusted from the value 520 ms reported in (*1*) to the pure extravascular fraction of the tissue) we obtain a relaxation time greater than 470 ms. This value is significantly larger than the value of 300 ms actually observed. The discrepancy implies that the fraction of nuclear spins affected by the contrast enhancement agent must be significantly larger than $f_{iv} = 0.07$. One can conclude that the agent must also exert an influence on the spin–lattice relaxation of *extravascular* nuclei. An analysis of observations of phase relaxation times (*5*) in the presence of the agent Dy-DTPA leads to the same conclusion, i.e., that an agent, even though it is strictly localized in the intravascular space, must affect the magnetization of extravascular nuclei. The question arises as to how the influence of contrast enhancing agents can be exerted beyond the vascular walls. An answer to this question should apply to both spin–lattice and phase relaxation.

2.2. Critique of a Model by Villringer et al. (5)

Villringer *et al.* (*5*) suggested that due to its paramagnetic properties Dy-DTPA induces inhomogeneous fields around blood vessels which lead to a dephasing of nuclear spins. This model cannot explain, however, an enhancement of spin–lattice relaxation since this kind of relaxation should not be affected very much by diffusion in a field gradient. That assumption can readily be verified for the experiments of Schmiedl *et al.* (*1*).

For the concentrations of albumin-(Gd-DTPA)$_{18}$ which these authors used one can estimate by means of the laws of magnetostatics (*9*) that the inhomogeneous field around the vessel has a magnitude of less than $10^{-7}B$ where B denotes the external field. Taking into account that the fastest spin–lattice relaxation rate is achieved when the perturbing field $B_{per} = \gamma\omega_{per}$ occurs with the Larmor frequency, $(1/T_1)_{max} = \frac{1}{2}(\langle\omega_{per}^2\rangle/\omega_L)$ (*10*), one concludes for an external field of 1 T that the relaxation rate is in the range of 10^{-6} s^{-1}. This rate is much smaller than the observed rate $T_1^{-1} > 1$ s^{-1} (*1*).

[1] $M(t)$ is considered to be normalized, i.e., $M(t = 0) = 1$.

In the next section we describe a model which satisfactorily explains enhancement of spin–lattice and phase relaxation of extravascular nuclear spins.

2.3. Exchange-Diffusion Mechanism

The model which we suggest is based on the assumption that nuclear spins (water protons) exchange between intra- and extravascular space. The vascular contrast agents rapidly relax the magnetization of the intravascular spins. However, diffusion across the vascular wall will mix intravascular and extravascular spins, such that after a while spins relaxed through the presence of the intravascular contrast agent will appear in the extravascular space. As a result the whole population of nuclear spins will exhibit relaxation enhancement. It is obvious that the suggested mechanism applies to both spin–lattice and phase relaxation.

The mechanism suggested has been investigated also by other authors in different settings. An example involved exchange of water protons across the erythrocyte membrane. A corresponding theory had been provided and applied by Conlon and Oethred (*11*) and reviewed by Morariu and Benga (*12*). These authors assumed, however, first order kinetics for the exchange across the erythrocyte membrane. In our description, in contrast, the exchange is described by the diffusion equation. We identify, in particular, an inhomogeneous distribution of magnetization near compartmental boundaries and a dependence of the exchange process on the volumes of the compartments and on diffusion to the compartment walls.

The degree to which the suggested mechanism affects relaxation times of extravascular magnetization depends on two conditions: (i) the exchange time across the vessel wall must be sufficiently small compared to the native (i.e., without presence of contrast agents) relaxation time of extravascular nuclear spins; (ii) the vessels must have a sufficiently high density in tissue; we will quantify below what criterion determines such densities. Condition (ii) ensures that a discernable fraction of extravascular magnetization is affected by the intravascular agents. Blood vessels which satisfy the above conditions are capillaries in the body tissue. The reason is that capillaries have the thinnest vascular walls (0.2–1 μm) (*13*), exhibit a maximal exchange surface between intra- and extravascular space, and have the highest density of all blood vessels in tissue [e.g., the intercapillary distance in heart measures 20–25 μm (*14*)].

Let us first estimate the transport time across the capillary wall, in order to demonstrate that condition (i) is satisfied for capillary vessels. Measured permeability coefficients of capillary walls (*8, 15, 16*) allow one to estimate an effective diffusion coefficient D_e in the capillary wall of 0.005–1 $\mu m^2\ ms^{-1}$. A rough estimate for the transition time τ_e to cross a capillary wall of thickness R_e is $\tau_e \approx R_e^2/D_e$ which yields transition times τ_e 1–500 ms which are well in the range of transition times across membranes of *in vitro* liposome systems (*17*). Since typical relaxation times at fields of 1 T in tissue are in the range 50–150 ms for phase relaxation (T_2), and in the range 200–800 ms for spin–lattice relaxation (T_1) (*18*), the first condition obviously is satisfied.

In order to consider in how far condition (ii) is satisfied we need to estimate over which distance d extravascular spins can diffuse within the native relaxation times toward and away from the vascular walls to get the fraction f of spins being affected

by diffusion-mediated relaxation: according to arguments presented in detail further below it holds $f \sim ((d + R_c)/\text{intervascular distance})^2$, where R_c is the capillary radius which measures about 3 μm (*19*). The diffusion constants in extravascular tissue are approximately 1–1.5 $\mu m^2/ms$ (*20*). Using the rough estimate $d \sim \sqrt{D \cdot \tau_{native}}$ where τ_{native} is the native nuclear spin relaxation time, i.e., either T_1 or T_2, and D the diffusion coefficient in the extracapillary medium, one obtains $d \geqslant 7$ μm and for the ratio $((d + 3\ \mu m)/\text{average intercapillary distance})^2$ a value greater than 0.16. This value is an estimate for the fraction of spins affected by relaxation. This value, which we consider to be a lower limit to the actual value, appears to be high enough for diffusion-transmitted relaxation to be discernable.

2.4. Model for Contrast Enhancement in Capillary Systems

For an exact description of the influence of contrast agents on nuclear spin relaxation in tissue a realistic capillary architecture of a specific tissue should be considered. Knowledge about transport parameters (diffusion coefficients) and relaxation rates of nuclear spin would be required for every point in the tissue. The consideration of that much detail in a mathematical model would result in an extremely cumbersome description. The aim of this paper is to study the principles behind the action of contrast enhancing agents rather than simulate specific tissue situations. For this reason we will study in the following a model which appears to be generic to the circumstances under which tissue contrast enhancement by means of intravascular agents develops. This model is defined by the following assumptions

1. Only the water proton fraction of nuclear spins is considered. This is justified as this fraction is clearly dominating in most tissues (*8*).

2. The initial nuclear magnetization is assumed to be homogeneous throughout the whole tissue volume considered. Since the initial magnetization is proportional to water proton concentration, and since the water proton concentration is nearly homogeneous in most tissues (*8*), the assumption made appears to be realistic.

3. Only three different compartments in a tissue are distinguished: (i) an intracapillary space in which the contrast agent is residing, (ii) a capillary wall, and (iii) extracapillary tissue. In each compartment the diffusion coefficient and the relaxation rate of nuclear spins are assumed to be constant. The latter implies that diffusion across cellular boundaries in the extracapillary tissue is rapid, such that one does not need to distinguish between intracellular and extracellular spaces. The magnetic field is supposed to be homogeneous in the whole tissue.

4. The capillaries are considered as long parallel cylinders. This geometry holds approximately in skeletal muscle, in heart, and in certain areas of brain (*14*). Each capillary is assigned the tissue volume (supply area), which is predominantly supplied by the capillary under consideration. According to the assumed capillary geometry the supply areas form concentric cylinders around the capillaries. Figure 1 shows a section through two adjacent capillaries. The radius of a cylindrical supply area will be referred to as the supply radius R_v. To determine R_v we consider a tissue with several capillaries all running parallel and the cross section perpendicular to the axis of the capillary cylinders. If there are n capillaries intersecting a cross section of area A, the supply radius is determined by $\pi R_v^2 = A/n$, i.e., $R_v = \sqrt{A/(\pi n)}$. $2R_v$ corresponds to the average intercapillary distance.

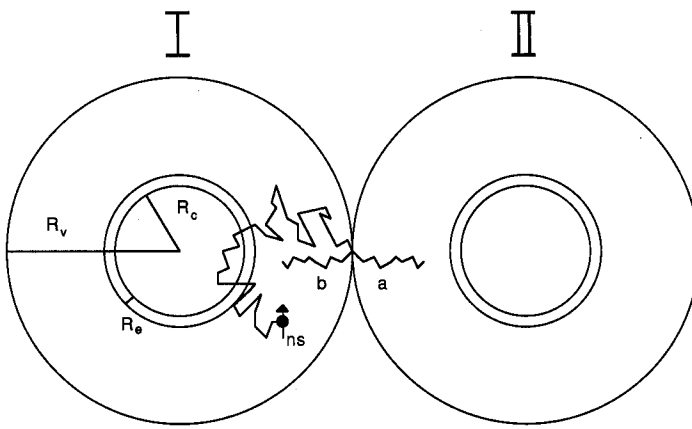

FIG. 1. View of two parallel capillaries (cross section) with supply areas denoted by I and II. R_c is the capillary radius, R_e the thickness of the capillary wall, and R_v the supply radius. A sample trajectory (a) of a nuclear spin (ns) which leaves supply area I and enters supply area II is shown. In our model we replace trajectory (a) by trajectory (b) which is identical to (a), except that the trajectory is reflected at the boundary of supply area I.

5. We assume that any nuclear spin will interact with only one capillary, the capillary closest to the spin's initial position. This assumption implies that if the trajectory of a nuclear spin leaves the supply area of capillary I and enters the supply area of capillary II, we replace this trajectory by a trajectory that is reflected at the boundary between the supply areas of capillary I and capillary II, actually returning then to capillary I. Such a trajectory is presented in Fig. 1. The diffusion of nuclear spins around capillaries is then described by a diffusion equation with reflective boundary conditions at the supply radius R_v.

2.5. Mathematical Analysis

We will now derive an expression for the relaxation time of nuclear magnetization around a capillary vessel which contains contrast enhancing agents. The derivation will be based on assumptions (*1–5*) above. The relaxation time obtained will depend on transport parameters (diffusion coefficients D_c, D_e, D_v in the three compartments, i.e., capillary vessel, capillary wall, and extracapillary space, on the average intercapillary distance, i.e., on capillary density, and on the relaxation times of nuclear spins T_c, T_e, T_v in the three tissue compartments. R_c denotes the capillary radius, R_e the thickness of the capillary wall, and R_v the supply radius of the capillaries (see Fig. 1).

We assume that a diffusion coefficient $D(\mathbf{x})$ accounts for stochastic transport of nuclear spins in a tissue at location $\mathbf{x} = (x_1, x_2, x_3)$. We further assume that the x–y-magnetization of spins is subject to phase relaxation with local rate $T_2^{-1}(\mathbf{x})$, and that the z-magnetization is subject to spin–lattice relaxation with local rate $T_1^{-1}(\mathbf{x})$. The local magnetization is then governed by the diffusion-Bloch equations (*21*),

$$\partial_t m_{x-y}(\mathbf{x}, t) = \left(\nabla \cdot D(\mathbf{x})\nabla - \frac{1}{T_2(\mathbf{x})} - i\omega(\mathbf{x})\right) m_{x-y}(\mathbf{x}, t), \qquad [2.1]$$

$$\partial_t m_z(\mathbf{x}, t) = \left(\nabla \cdot D(\mathbf{x})\nabla - \frac{1}{T_1(\mathbf{x})}\right) m_z(\mathbf{x}, t). \qquad [2.2]$$

In our model we consider the magnetic field in tissue to be homogeneous. This corresponds to a spatially independent Larmor frequency ω. The corresponding term in [2.1] leads to a multiplication of the x–y-magnetization by a phase factor $e^{-i\omega t}$. Redefining $m = e^{-i\omega t} \cdot m_{x-y}$, both Eqs. [2.1] and [2.2] can be written

$$\partial_t m(\mathbf{x}, t) = \left(\nabla \cdot D(\mathbf{x})\nabla - \frac{1}{T(\mathbf{x})}\right) m(\mathbf{x}, t), \qquad [2.3]$$

where $m(\mathbf{x}, t)$ describes either the x–y-magnetization or the z-magnetization, and where $T^{-1}(\mathbf{x})$ describes the spatially dependent phase relaxation rate or spin–lattice relaxation rate of a nuclear spin, respectively.

For the initial condition we assume a constant magnetization in the whole tissue, i.e.,

$$m(\mathbf{x}, t = 0) = m_0. \qquad [2.4]$$

The flux of magnetization $D(\mathbf{x})\nabla m(\mathbf{x})$ in [2.3] is coupled to the transport of nuclear spins and, hence, of particles. At the boundaries between the different compartments of tissue defined above, the flux component normal to the compartment boundaries must be continuous, otherwise particles would be generated or destroyed at these boundaries. The tissue compartments have cylindrical symmetry around the capillary axis. Conditions for the radial components of the flux, i.e., for $j_r = D(r)\partial_r m(r, t)$ result from this property. At the boundary between the intracapillary space and the capillary wall the continuity condition,

$$D_c \partial_r m_{:r \to R_c, r < R_c} = D_e \partial_r m_{:r \to R_c, r > R_c}, \qquad [2.5]$$

holds, and similarly at the boundary between the capillary wall and the extracapillary space holds

$$D_e \partial_r m_{:r \to R_c + R_e, r < R_c + R_e} = D_v \partial_r m_{:r \to R_c + R_e, r > R_c + R_e}. \qquad [2.6]$$

Spatial boundary conditions need to be envoked also at $|\mathbf{x}| = R_v$. The conditions result from the assumption of our model that particle trajectories are reflected when they attempt to enter the supply area of a neighboring capillary vessel, i.e., that no net magnetization is transported across the boundary $|\mathbf{x}| = R_v$. This assumption implies the condition

$$D_v \partial_r m(R_v, t) = 0. \qquad [2.7]$$

To account for the symmetry we employ cylindrical coordinates which render Eq. [2.3] in the form

$$\partial_t m(r, t) = \left(\frac{1}{r}\partial_r r D(r) \partial_r - \frac{1}{T(r)}\right) m(r, t),$$

$$= \mathbf{L} m(r, t). \qquad [2.8]$$

where the operator $\mathbf{L} = ((1/r)\partial_r(r \cdot D(r)\partial_r) - (1/T(r))$ is restricted to a function space characterized by the conditions [2.5], [2.6], and [2.7]. The formal solution of Eq. [2.8] is given by the expression

$$m(r, t) = \exp(t\mathbf{L})m_0. \qquad [2.9]$$

The mean local rate of relaxation $T_{\text{relax}}^{-1}(\mathbf{x})$ is the rate which approximates best the relaxation of the local magnetization by a single exponential decay (*10*), i.e., $m(\mathbf{x}, t) \approx m_0 \exp(-t/T_{\text{relax}}(\mathbf{x}))$. This approximation corresponds to the mean relaxation time approximation for the time development of $m(\mathbf{x}, t)$ and can be systematically improved (*22*). The criterion for the optimal match between the monoexponential approximation implied by a single relaxation time and the exact decay of observables has been investigated in (*22*) and references therein. The criterion for the optimal match is that the approximation reproduces the exact initial value as well as the time integral over the exact solution. The latter condition implies

$$T_{\text{relax}}(\mathbf{x}) = \int_0^\infty \frac{m(\mathbf{x}, t)}{m_0}\, dt, \qquad [2.10]$$

from which follows

$$\mathbf{L}T_{\text{relax}}(r) = -\mathbf{e}. \qquad [2.11]$$

$\mathbf{e}$ is the function which assumes the value 1 everywhere in the supply region.

Since we assumed constant values $D(r)$ and $T(r)$ for each tissue compartment, Eq. [2.11] in each compartment is piecewise equivalent to

$$\left(\frac{1}{r} D_i \partial_r(r\partial_r) - \frac{1}{T_i}\right) T_{\text{relax}}(r) = -1, \qquad [2.12]$$

where the index i denotes the compartment, i.e., i = c, e, v.

The mean relaxation time of the overall nuclear magnetization $M(t) = \int_V m(\mathbf{x}, t)d\mathbf{x}^3$ is determined by the spatial average of the local mean relaxation time T_{relax} over the diffusion space V,

$$T = \langle T_{\text{relax}}(\mathbf{x})\rangle_V = \frac{1}{\pi R_v^2} \int_0^{R_v} T_{\text{relax}}(r) \cdot 2\pi r dr. \qquad [2.13]$$

2.6. Results

In this section we discuss some typical features of the model developed above. For this purpose we investigate the dependence of the local mean relaxation time $T_{\text{relax}}(\mathbf{x})$ and of the global mean relaxation time $T = \langle T_{\text{relax}}(\mathbf{x})\rangle_V$ on the supply radius and on the permeability of the capillary wall. For the determination of the local mean relaxation time $T_{\text{relax}}(\mathbf{x})$ the differential equation [2.12] has been solved numerically by the *shooting method* (*23*), taking the boundary conditions [2.5]–[2.7] into account. The global mean relaxation time was then determined by numerical integration [*Simpson method* (*23*)] of the local mean relaxation time according to Eq. [2.13].

The relaxation times of nuclear spins in the extracapillary space, T_e and T_v, were chosen to be 50 ms, i.e., equal to typical phase relaxation times in muscle tissue (*18*).

The intracapillary relaxation time T_c was chosen very short, i.e., 5 ms, to demonstrate the effect of rapid intracapillary phase relaxation.

The local mean relaxation time T_{relax} in the vicinity of a capillary having a supply radius of 15 μm is shown in Fig. 2 for four effective diffusion coefficients D_e of the capillary wall. The smaller D_e the larger is the difference between intra- and extracapillary mean relaxation time. This is due to the fact that relaxation of the extracapillary nuclear magnetization develops when nuclear spins that have lost their magnetization in the intracapillary space pass from intra- to extracapillary space. The flow of nuclear spins leaving the intracapillary space is determined by the time τ_e needed by a nuclear spin to pass the capillary wall. τ_e is a function of the effective diffusion coefficient D_e and of the thickness R_e of the capillary wall. The estimate suggested above $\tau_e \approx R_e^2/D_e$ for $R_e = 0.2$ μm and $D_e = 0.1$ $\mu m^2/ms$ yields a value $\tau_e \approx 0.4$ ms. An effective wall diffusion coefficient $D_e = 0.005$ $\mu m^2/ms$ leads to a transit time which is 20 times longer, i.e., the effect of enhanced intravascular relaxation on the decay of extravascular magnetization would be much smaller in this case.

If one changes τ_e by variation of the capillary wall thickness one finds that an increase of this thickness and, hence, an increase of τ_e, enlarges the difference between intra- and extracapillary mean relaxation time. This effect is demonstrated by the results presented in Fig. 3.

When the supply radius R_v increases, i.e., capillary density decreases, the global mean relaxation time T becomes longer. This behavior is shown in Fig. 4 which

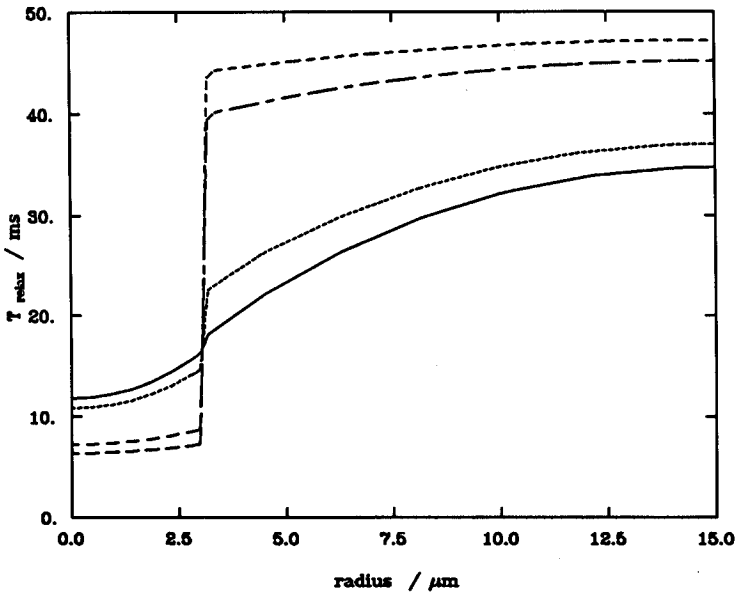

FIG. 2. Dependence of the mean local relaxation time $T_{relax}(r)$ of local nuclear magnetization $m(r, t)$ on the distance r from the capillary axis; $T_{relax}(r)$ has been evaluated according to Eq. [2.12] and is shown for four different diffusion coefficients: $D_e = 0.5$ $\mu m^2/ms$ (—), 0.1 $\mu m^2/ms$ (-------), 0.01 $\mu m^2/ms$ (— — — —), and 0.005 $\mu m^2/ms$ (- - -). Other constants assumed are $D_c = D_v = 1.5$ $\mu m^2/ms$, $R_c = 3$ μm, $R_e = 0.2$ μm, $R_v = 15$ μm, $T_c = 5$ ms, $T_e = T_v = 50$ ms.

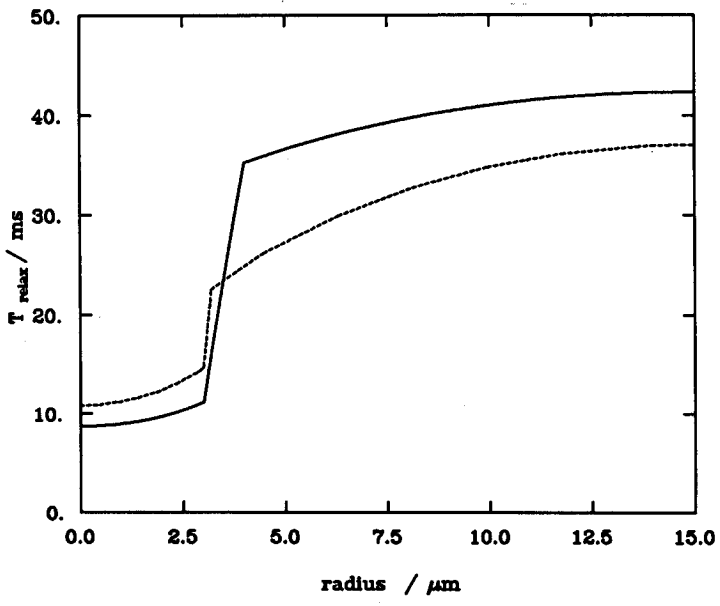

FIG. 3. Dependence of the mean local relaxation time $T_{relax}(r)$ on the distance r from the capillary axis. Two different wall thicknesses R_e have been assumed, $R_e = 0.2$ µm (-------) and $R_e = 1.0$ µm (—). The diffusion coefficient D_e in the capillary wall had been chosen to be 0.1 µm²/ms. Other parameters are the same as in Fig. 2.

represents the global relaxation rate as a function of R_v. An increased supply radius implies longer diffusion from the intracapillary space to the periphery of the supply region. The nuclear spins traveling this enlarged distance need a longer diffusion time. Thus, the influence of nuclear spin exchange between intra- and extracapillary space on relaxation enhancement of extracapillary nuclear magnetization decreases, i.e., the mean relaxation time increases.

The permeability of the capillary wall is determined by the effective diffusion coefficient D_e and by the thickness of the wall R_e. If the permeability of the capillary wall decreases by reduction of the effective diffusion coefficient D_e or by enlargement of the wall diameter R_e, the global mean relaxation time increases. The effect of D_e and R_e on the global relaxation rate is shown in Figs. 5 and 6, respectively. The effect demonstrated in these two figures can be explained as follows: decreased permeability of the capillary wall reduces the exchange between intra- and extracapillary nuclear spins; this causes a reduced relaxation of extracapillary nuclear magnetization and, hence, lengthens relaxation time.

2.7. Possible Diagnostic Application

Our exchange-diffusion model above gives a better understanding of the processes in tissue leading to pathological deviations of relaxation rates in the presence of contrast agent. This may allow one to develop new strategies for earlier as well as better classification of pathological tissue. As a first attempt to correlate the theory developed

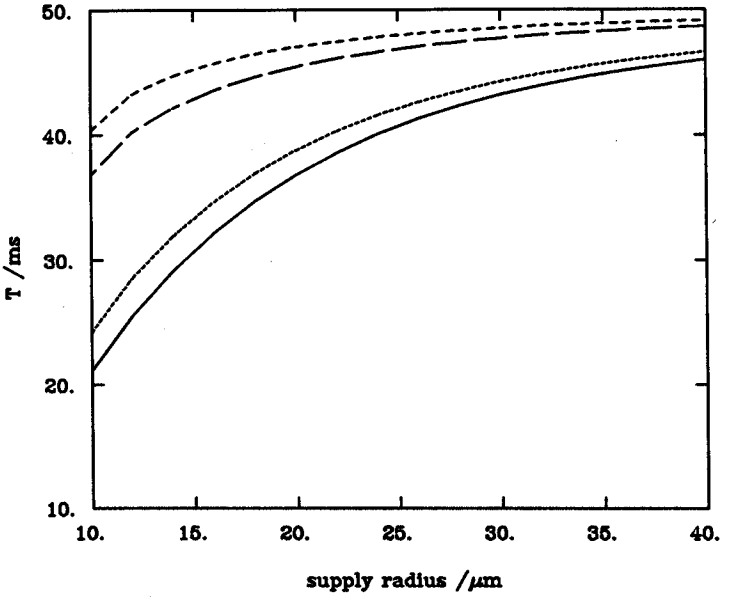

FIG. 4. Dependence of the global mean relaxation time T on the supply radius R_v. T has been evaluated according to Eq. [2.13] and is shown for four different diffusion coefficients D_e: 0.5 $\mu m^2/ms$ (—), 0.1 $\mu m^2/ms$ (-------), 0.01 $\mu m^2/ms$ (– — – —), and 0.005 $\mu m^2/ms$ (– – –). Other parameters are the same as in Fig. 2.

with data we have analyzed contrast enhancement in *in vitro* liposome systems. Such systems contain, for example, contrast agent confined to the liposome interior, yet exhibit increased relaxation rates of bulk water in the region exterior to the liposome particles (*17*). In the following we will use the terms *enhanced* and *reduced relaxation rates* to imply a comparison between normal tissue and tissue with contrast agent.

We first consider the common disease arteriosclerosis. Arteriosclerosis is distributed over multiple arterial systems, e.g., the coronary arteries. The density of capillaries in the tissue area, which is supplied by an affected artery, decreases up to 20% (*24*). To describe this situation by our model one needs to assume an increased intercapillary distance. According to the results presented above (see Fig. 4) the relaxation rate in this case is reduced. If we now assume that our model is relevant for heart tissue we can conclude that the pathological tissue should exhibit reduced (with respect to normal heart tissue) relaxation rates and, therefore, should reveal itself through a contrast difference.

Another disease accompanied by reduced density of capillaries is hypertrophy of the heart muscle which occurs as a consequence of arterial hypertension (*25*) or as a compensatory mechanism in the surviving myocardium after infarction (*26*). In normal muscle each capillary has a well-defined supply area. During hypertension muscle fibers between the capillaries enlarge whereas the total number of capillaries remains the same (one capillary/one muscle fiber) (*24*), i.e., the density of capillaries decreases by, 17–20% (*26*), or by 30% (*27*). The supply radius of single capillaries increases

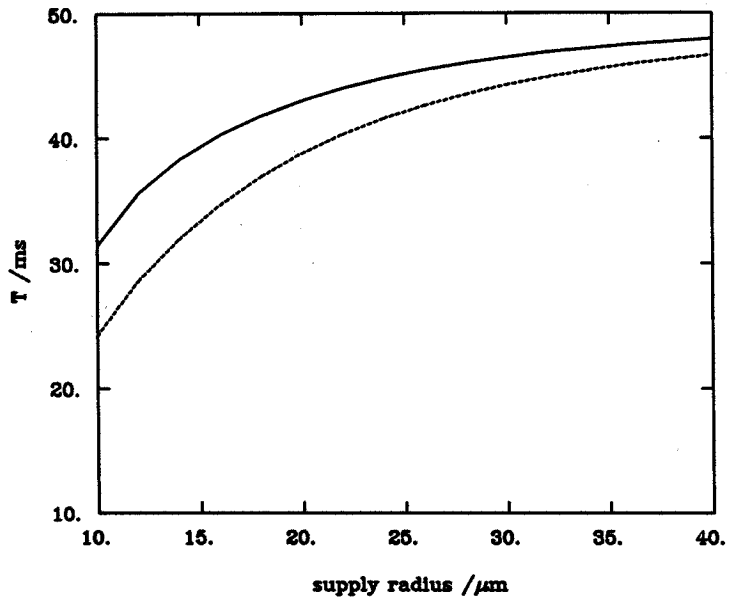

FIG. 5. Dependence of the global mean relaxation time T on the supply radius R_v for two different sizes of the capillary wall, $R_e = 1.0$ μm (-------) and $R_e = 0.2$ μm (—). The diffusion coefficient in the capillary wall, D_e, had been chosen to be 0.1 $\mu m^2/ms$. Other parameters are the same as in Fig. 2.

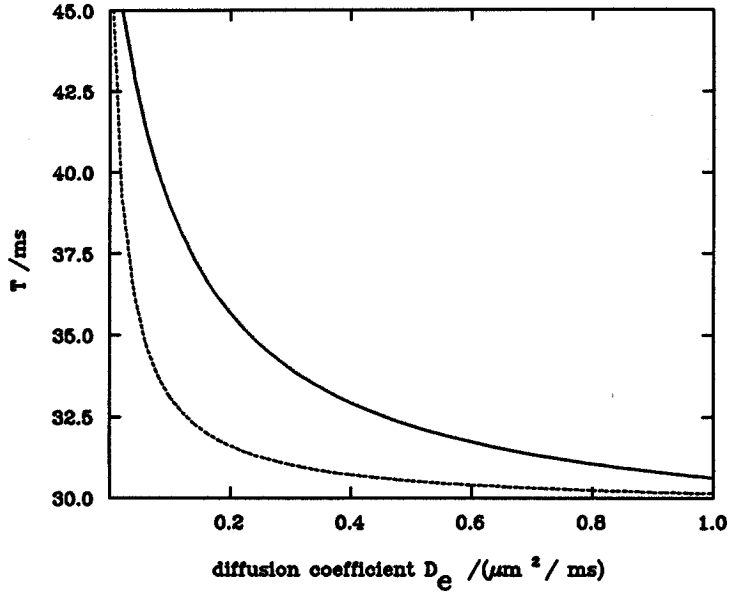

FIG. 6. Dependence of the global mean relaxation time T on the capillary wall diffusion coefficient D_e for a wall size $R_e = 1.0$ μm (-------) and $R_e = 0.2$ μm (—). Other parameters are the same as in Fig. 2.

and the peripheral regions of the supply areas suffer from decreased nutrition (*25, 28*). As a result, the contractility of the heart decreases and the heart develops insufficiency (*24*). This disease provides an excellent example to illustrate (i) the physiological meaning of the supply area introduced, and (ii) the role of transport from intra- to extracapillary space. According to the results obtained for the diffusion-exchange model, the enlarged supply radius leads to a reduction of the relaxation rates in the affected heart tissue.

Examples of tissues with increased number of capillaries are certain tumor tissues (*29*). Most tumors expand rapidly and consequently require enhanced metabolism. This can only be achieved by increasing the density of capillaries in the tumor (*29*). According to the results of our model the relaxation rates should be increased. However, often one observes also the opposite behavior. This arises due to a degradation of tissue in the necrotic core of a tumor which is then devoid of any capillaries and hence of contrast agent.

In the following we consider pathological states which we assume to influence the permeability of the capillary wall. Since such influence cannot as yet be proven our conclusions contain a strong element of speculation. Although morphological alterations of capillary walls have been observed in certain pathological tissues, it has not been shown that these alterations are accompanied by altered transport properties. The reason is that until now it has often been impossible to study transport in tissue under physiological conditions, especially *in vivo*. NMR imaging methods might, in fact, be used to prove that transport is an important factor of the pathological states of certain diseases.

A disease which changes the morphology of capillary walls is diabetes (*microangiopathia diabetica*). The *lamina basalis* of the capillaries involved becomes thicker and the endothelia cells suffer from destruction (*30*). Assuming that this development of the tissue is due to poor supply, these symptoms make it appear probable that the permeability of the capillary walls is reduced in *microangiopathia diabetica*. According to the diffusion-exchange model a decrease of capillary wall permeability enhances the relaxation time of the tissue, i.e., it should be observable by MRI.

Oedema after intoxication, allergy, or trauma is caused by increased permeability of the capillary wall (*24*). In following the results of the diffusion-exchange model one expects a decreased relaxation time and an enhanced contrast in the affected tissue.

3. CONTRAST ENHANCEMENT BY MAGNETIC PARTICLES

In this section we investigate the mechanism of contrast enhancement by magnetic particles in Kupffer cells of liver. We will show that transport of nuclear spins to Kupffer cells is likely to be the origin for contrast in liver. Our discussion leads to the suggestion of a model describing enhanced relaxation rates around Kupffer cells by a diffusion-reaction mechanism. A formula is derived which reveals the dependence of the relaxation rate on the concentration of Kupffer cells in liver. The latter is important as no other means of measuring the concentration is available. We will also discuss to what extent the relaxation rate, as observed in MRI, can be used for diagnosis of liver diseases.

3.1. *Ferromagnetic Particles in Kupffer Cells*

Ferromagnetic and superparamagnetic substances recently used for contrast enhancement of liver (*2*) are magnetite particles $Fe_2^{3+}O_3 \cdot Fe^{2+}O$ of size 0.5–1.0 μm or smaller. These contrast agents are injected into a vein and, after a certain period, become deposited mainly in liver, spleen, and bone marrow. Histological examination of liver reveals that the particles are present only in Kupffer cells, macrophages of liver, whereas the parenchymal cells, e.g. hepatocytes in liver, remain free from contrast agent (*2*). Thus, the effect of contrast enhancement is connected with the presence of Kupffer cells.

This latter feature is important for diagnosis since Kupffer cells can serve as markers for pathological processes in liver. Hepatitis and chronic alcohol abuse are accompanied by an enhanced number of Kupffer cells (*29*). In liver metastasis and liver carcinoma the number of Kupffer cells is reduced with respect to normal (*31*). Based on this fact Saini *et al.* (*31*) showed that after application of magnetic particles focal liver carcinoma could be distinguished well from normal liver tissue by observing differences of contrast enhancement in liver. Thus, a model describing contrast enhancement as a function of the density of Kupffer cells could be very useful for diagnosis of liver diseases as long as other changes in the tissue are not more important in affecting local relaxation rates. Before we develop such a model we review first the mechanism of contrast enhancement in liver due to magnetic particles in Kupffer cells.

3.2. *Relaxation Enhancement by Magnetic Field Inhomogenities*

Contrast enhancement of liver by magnetic particles originates from reduction of phase relaxation time T_2 (*2*). Since the spin–lattice relaxation time T_1 is only rarely affected (*2*), enhancement of the phase relaxation rate T_2^{-1} should be mainly due to enhancement of the secular part of T_2^{-1} (*20*).[2] The secular part of the phase relaxation rate is determined by stochastic modulation of the precession frequency of a nuclear spin (*20*) which occurs when precessing nuclear spins diffuse in an inhomogeneous magnetic field, the latter being parallel to the external field. In the presence of an external magnetic field superparamagnetic particles have the property to acquire very large magnetic moments which can induce strong inhomogeneous magnetic fields around Kupffer cells (*2*). Hence, nuclear spins which diffuse in the proximity of Kupffer cells rapidly lose their transverse magnetization.

We want to consider now the spatial dependence of nuclear relaxation enhancement around a Kupffer cell. As enhanced phase relaxation is due to diffusion in an inhomogeneous magnetic field, a quantity describing the inhomogenity is required. This quantity is given by the gradient of the magnetic field component parallel to the external field, i.e., by the gradient of the space-dependent spin precession frequency $\mathbf{G} = \nabla\omega(\mathbf{x})$. A precessing nuclear spin which diffuses a distance $\delta\mathbf{x}$ in the gradient experiences a modulation of its Larmor frequency $\delta\omega = \delta\mathbf{x} \cdot \mathbf{G}$. The larger the gradient

[2] This conclusion can be derived from the fact that T_2^{-1} can be decomposed into a secular and into a nonsecular contribution (*20*), $T_2^{-1} = T_{2,\text{secular}}^{-1} + T_{2,\text{nonsecular}}^{-1} \cdot T_{2,\text{nonsecular}}^{-1}$ is due to spin flip processes, i.e., the same processes as involved in spin–lattice relaxation. Hence, $T_{2,\text{nonsecular}}^{-1}$ and T_1^{-1} have the same magnitude (*10*).

the more pronounced is the variation of the Larmor frequency and, hence, the faster nuclear spins lose their transverse magnetization (*20*).

In the following we always assume that the external field is parallel to the z-direction. If the gradient were constant, the transverse magnetization m_{x-y} would decay as $m_{x-y}(t) = f \cdot m_{x-y}(t = 0)$, where f is the factor

$$f = \exp\left(-\frac{1}{3} D|\mathbf{G}|^2 t^3\right), \qquad [3.1]$$

and where D is the diffusion constant (*21*). As can be seen from Eq. [3.1], the quantity describing phase relaxation is the square of the gradient $\mathbf{G}$.

The magnetic field around Kupffer cells can be approximated by a dipole field (*20*), i.e., the spatially dependent Larmor frequency can be written in spherical coordinates ($\mathbf{x} = (r, \vartheta)$) as (*32*)

$$\omega(r, \vartheta) = \gamma\mu_z \frac{\mu_0}{4\pi} \cdot \frac{3\cos^2\vartheta - 1}{r^3}, \qquad [3.2]$$

where μ_z is the dipole moment of the Kupffer cell, μ_0 is the magnetic permeability, and γ is the gyromagnetic ratio. μ_z is proportional to the amount of magnetic material stored in a Kupffer cell. The square of the gradient is

$$|\mathbf{G}(r, \vartheta)|^2 = \frac{1}{r^8} \cdot 9(1 - 2\cos^2\vartheta + 5\cos^4\vartheta)\left(\gamma\mu_z \frac{\mu_0}{4\pi}\right)^2. \qquad [3.3]$$

To derive an approximation for the transverse magnetization decay around Kupffer cells, we consider, $|\mathbf{G}(r, \vartheta)|^2$, to be the relevant quantity. Eq. [3.3] reveals that due to the radial dependence r^{-8} of $|\mathbf{G}(r, \vartheta)|^2$ the relaxation develops near the Kupffer cell, and the effect of magnetite decays rapidly with increasing distance from the Kupffer cell.

3.3. Diffusion–Reaction–Mechanism

We suggest that the enhanced phase relaxation of nuclear magnetization spreads around Kupffer cells through diffusion. To describe this relaxation we divide the space around a Kupffer cell into two subspaces. The first subspace, which we will refer to as the *effect volume,* is adjacent to the Kupffer cells. A magnetized nuclear spin entering this volume will experience instant relaxation. The second subspace is the *complementary space* to the effect volume. In this subspace the influence of Kupffer cells on phase relaxation of a nuclear spin is neglected. Hence, the overall phase relaxation will depend on the rate with which nuclear spins enter the effect volume. This rate itself is a function of the density of Kupffer cells and of the geometry of the effect volume. Since the demagnetization ("reaction") of a nuclear spin takes place only in the effect volume around a Kupffer cell and the rate with which spins enter the effect volume is diffusion controlled, the term *diffusion-reaction model* is used for our description.

3.3.1. Definition of the effect volume. The fast decrease of nuclear phase relaxation with increased radius as described by Eq. [3.3] suggests that a division into two complementary subspaces, the effect volume, in which nuclear spins instantaneously lose

transverse magnetization, and the complementary volume, in which an influence of the magnetic substance is neglected, should provide an adequate description. The boundary between the effect volume and the complementary volume is determined by a critical gradient G_c, the magnitude of which is the threshold above which an influence of the magnetic field surrounding a Kupffer cell is accounted for, i.e., G_c should induce a relaxation of nuclear spins which is very fast compared to the native relaxation.

The surface Ω_c of the effect volume is defined as the set of points x which satisfy

$$|\mathbf{G}(r, \vartheta)| = G_c. \qquad [3.4]$$

According to Eq. [3.3] this implies the condition

$$\frac{1}{r^8} \cdot 9(1 - 2\cos^2\vartheta + 5\cos^4\vartheta)\left(\gamma\mu_z \frac{\mu_0}{4\pi}\right)^2 = G_c^2. \qquad [3.5]$$

The critical gradient separates volumes with high and small phase relaxation rate, a behavior which, in our model, is replaced by a discontinuity in the local relaxation rates. Such discontinuity is certainly an oversimplification and should provide a description which is the better, the faster $|\mathbf{G}(r, \vartheta)|^2$ decays in going from the effect volume to the complementary volume. In order to investigate this decay we consider the gradient $\partial_r|\mathbf{G}(r, \vartheta)|^2$ at the surface Ω_c of the effect volume, Ω_c being defined through Eq. [3.5]. From this equation and from Eq. [3.3] one can derive

$$\partial_r|\mathbf{G}|^2_{\mathbf{x}\in\Omega_c} = -8 \cdot |\mathbf{x}|^{-1} \cdot G_c^2. \qquad [3.6]$$

Equation [3.6] demonstrates that our assumption of a discontinuous jump in $|\mathbf{G}|^2_{\mathbf{x}\in\Omega_c}$ holds better for smaller effect volumes ($|\mathbf{x}|$ small).

Unfortunately, even after the assumption of the defined effect volume surrounding Kuppfer cells, the resulting model is still not amenable to an analytical mathematical description. The reason is that the surface Ω_c is too complicated. However, Ω_c deviates actually only very little from a spherical surface, a shape, for which the system can be described more readily. In order to show that Ω_c is almost spherical we note first that the distance of Ω_c from its center ($r = 0$) is smallest for the angles $\vartheta_1 = 0, \pi$ and largest for the angles defined through $\cos(\vartheta_2) = 0.2$, the smallest and largest distances being $r_1 = r(\vartheta_1)$ and $r_2 = r(\vartheta_2)$. From Eq. [3.5] one can determine that the ratio r_2/r_1 has the value 1.2. This value is close enough to "1" to allow us to replace Ω_c by a spherical surface.

We defined the radius of the spherical effect volume as the mean value of the radius $r(\vartheta)$ over the angle ϑ, i.e., $R_e = \langle r(\vartheta)\rangle$. One obtains the value

$$R_e = \frac{1}{2}\int_0^\pi d\vartheta \sin\vartheta\, r(\vartheta)$$

$$= \beta\left(\gamma\mu_z \frac{\mu_0}{4\pi} \cdot \frac{1}{G_c}\right)^{1/4}, \qquad [3.7]$$

where β is

$$\beta = \frac{1}{2}\int_0^\pi d\vartheta \sin\vartheta \,(9\cdot(1 - 2\cos^2(\vartheta) + 5\cos^4(\vartheta)))^{1/8} \approx 1.35.$$

The small value of the standard deviation $\Delta = (\sqrt{\langle r^2(\vartheta)\rangle - \langle r(\vartheta)\rangle^2}/\langle r(\vartheta)\rangle) \approx 6\%$ implies that the above definition of R_e provides a close approximation to the surface of the exact effect volume. It is noteworthy that R_e in Eq. [3.7] depends solely on the ratio μ_z/G_c. We will assume later on that this quantity is proportional to the dose of the magnetic substance; this linear relationship can be expected to hold for low dose levels, i.e., when saturation effects can be discounted.

3.3.2. Model for enhanced phase relaxation around several Kupffer cells. A mathematical description of enhanced phase relaxation around Kupffer cells would still elude us if we needed to include, in an exact manner, the possibility that diffusing spins can interact with more than one Kupffer cell. However, one can rationalize that one needs to consider only situations in which spins interact with a single Kupffer cell. Encounters with second, third, . . . Kupffer cells are accounted for effectively by reflecting the trajectory of a spin, once it leaves a Kupffer cell to approach more closely a second Kupffer cell, back to the first Kupffer cell. This approach amounts to surrounding Kupffer cells with a spherical diffusion space, the radius of which measures half the medium distance between Kupffer cells. The diffusion space is limited at that radius by a reflective boundary described by a boundary condition as discussed in Sect. 2.5 above (see Eq. [2.7]).

Our model of enhanced phase relaxation around Kupffer cells involves then the following assumptions:

1. Only the water proton fraction of nuclear spins is considered.
2. The initial nuclear magnetization is assumed to be homogeneous in liver tissue.
3. The external magnetic field is supposed to be homogeneous outside the effect volumes of Kupffer cells.
4. The diffusion constant and the native phase relaxation rate in liver tissue are considered to be constant. This assumption may not apply in the presence of pathologies since the value of the diffusion coefficient in liver tissue is actually determined by the permeability of the membranes of hepatocytes.
5. We assume that any nuclear spin will interact only with the effect volume of a single Kupffer cell, the Kupffer cell closest to the spin's initial position. We, therefore, restrict the diffusion space to a sphere around the Kupffer cell. The volume of this spherical diffusion space is given by the mean tissue volume per Kupffer cell, i.e., the radius of the diffusion space R_a is determined by

$$R_a = \left(\frac{3}{4\pi c}\right)^{1/3}, \qquad [3.8]$$

where c is the density of Kupffer cells. $2R_a$ corresponds approximately to the mean distance between Kupffer cells. The assumption that diffusion of nuclear spins is restricted to a sphere with radius R_a implies that diffusion is described by a diffusion equation with reflective boundary conditions at the surface of this sphere. Thus, a magnetized nuclear spin diffuses inside a spherical diffusion space until the spin has reached the effect volume where it is demagnetized instantaneously. After this event

the nuclear spin "disappears" from consideration as it is only through nonvanishing magnetization $m(\mathbf{x}, t)$ that a spin can be observed.

3.4. Mathematical Analysis

We assume, in accordance with the NMR pulse sequence applied, homogeneous initial magnetization, i.e.,

$$m_{x-y}(\mathbf{x}, t = 0) = m_0. \tag{3.9}$$

According to the model suggested, the m_{x-y} component of nuclear spin magnetization vanishes instantaneously as spins enter the effect volume. This is expressed by the condition

$$m_{x-y}(\mathbf{x}, t) \equiv 0, \ |\mathbf{x}| \leqslant R_e, t > 0, \tag{3.10}$$

where R_e is the radius of the effect volume. The spatial boundary condition at the surface of the diffusion space is determined by the assumption that nuclear spins are reflected at this surface, the reasons being analogue to those given in Section 2. This implies the condition

$$\partial_r m_{x-y}(\mathbf{x}, t) \equiv 0, \ |\mathbf{x}| = R_a. \tag{3.11}$$

In the space $R_e < |\mathbf{x}| < R_a$ the local nuclear magnetization is governed by (*21*)

$$\partial_t m_{x-y}(\mathbf{x}, t) = \left(D\nabla^2 - i\omega_0 - \frac{1}{T_{2,0}} \right) m_{x-y}(\mathbf{x}, t), \tag{3.12}$$

where D is the diffusion constant, ∇^2 the Laplace operator, ω_0 the Larmor frequency, and $T_{2,0}^{-1}$ the native phase relaxation rate. Taking the spherical symmetry into account and defining $m = \exp(t(i\omega_0 + 1/T_{2,0})) \cdot m_{x-y}$ leads to the simple diffusion equation

$$\partial_t m(r, t) = D \frac{1}{r} \partial_r^2 (r m(r, t)). \tag{3.13}$$

The formal solution of Eq. [3.13] is

$$m(r, t) = \exp(t\mathbf{L}) m_0. \tag{3.14}$$

with $\mathbf{L} = (D(1/r)\partial_r^2 r)$. The relaxation rate $T_{\text{relax}}^{-1}(r)$ of the transformed local magnetization $m(r, t)$ is the rate which approximates best the relaxation of $m(r, t)$ by a single exponential decay, i.e., $m(r, t) \approx m_0 \exp(-t/T_{\text{relax}}(r))$ (*10*). The relaxation rate of the transformed magnetization $m(r, t)$ and the original magnetization $m_{x-y}(r, t)$ differ by the native phase relaxation rate $T_{2,0}^{-1}$. Thus, the rate T_{relax}^{-1} gives the increment of the relaxation rate in the presence of magnetic particles.

According to the *mean relaxation time approximation* (*22*) $T_{\text{relax}}(r)$ can be determined by an approach which is identical to the one adopted in Sect. 2.5, i.e., it holds

$$\mathbf{L} T_{\text{relax}}(r) = -\mathbf{e}.$$

Integration yields

$$T_{\text{relax}}(r) = -\frac{r^2}{6 \cdot D} + C_1 + \frac{C_2}{r}, \tag{3.15}$$

with C_1 and C_2 as constants to be determined according to the boundary conditions [3.10] and [3.11], i.e.,

$$C_2 = -\frac{R_a^3}{3 \cdot D}, \qquad [3.16]$$

$$C_1 = \frac{R_e^2}{6 \cdot D} + \frac{R_a^3}{3 \cdot D \cdot R_e}. \qquad [3.17]$$

The global mean relaxation time of the overall transformed magnetization $M(t) = \int_0^{R_a} m(r, t) 4\pi r^2 dr$ is the spatial average of $T_{relax}(r)$,

$$T = \frac{1}{(4/3)\pi R_a^3} \int_0^{R_a} T_{relax}(r) \cdot 4\pi r^2 dr. \qquad [3.18]$$

With $q = R_e/R_a$ one obtains

$$T = \frac{R_e^2}{D} \cdot F(q), \qquad [3.19]$$

where

$$F(q) = q^{-2}\left(-\frac{1}{10}(1 - q^5) + \frac{1}{3}\left(\frac{q^2}{2} + q^{-1}\right)(1 - q^3) - \frac{1}{2}(1 - q^2)\right). \qquad [3.20]$$

The global relaxation rate T^{-1} as a function of R_e/R_a is presented in Fig. 7. Since Eq. [3.8] relates the density of Kupffer cells c to the radius R_a of the diffusion space,

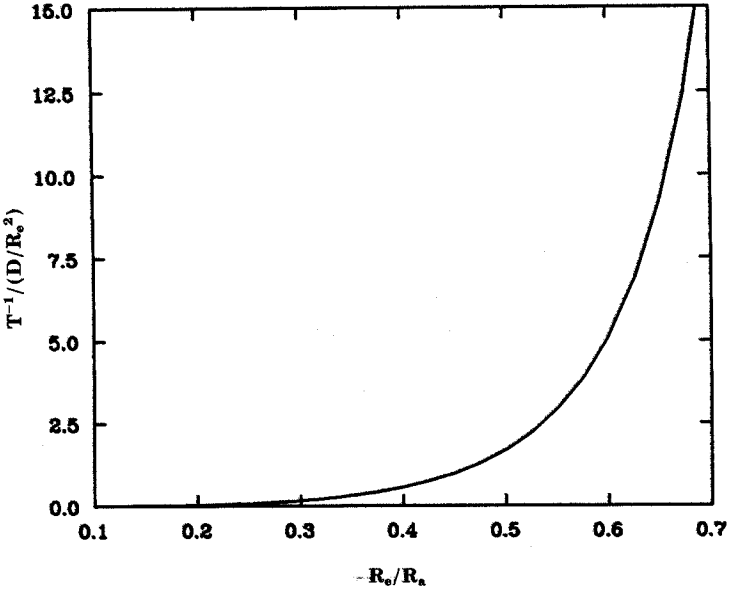

FIG. 7. Dependence of the (incremental) phase relaxation rate T^{-1} due to magnetic particles in Kupffer cells on the ratio R_e/R_a. T has been evaluated according to Eqs. [3.19] and [3.20].

the global relaxation time in Eq. [3.19] can be expressed also as a function of the density of Kupffer cells

$$T = \frac{R_e^2}{D} \cdot F\left(R_e \cdot \left(\frac{4}{3}\pi c\right)^{1/3}\right). \qquad [3.21]$$

When the radius of the effective volume R_e is much smaller than the mean distance between Kupffer cells, i.e., $q = R_e/R_a \to 0$, which obviously holds for very small intracellular concentrations of magnetic particles or widely spaced Kupffer cells, [3.19] can be written

$$T = \frac{1}{3}\frac{R_a^3}{DR_e}, \qquad [3.22]$$

and with the help of Eq. [3.8] one obtains

$$T^{-1} = 4\pi D R_e c. \qquad [3.23]$$

Equation [3.23] demonstrates that in the above-mentioned limit the relaxation rate is proportional to the density c of Kupffer cells in the tissue.

3.5. Application of the Model to Experimental Results

In this section we will apply our model to an experiment carried out by Saini *et al.* (*2*). Saini *et al.* observed NMR signal intensities as a function of the dose of magnetite iron. Since our model deals with relaxation rates we transform the observed signal intensities to relaxation rates.

After application of magnetic particles Saini *et al.* (*2*) observed a dose-dependent decrease of NMR signal intensity in liver. The signal intensities were produced by the spin-echo method with the pulse sequence parameters TR = 500 ms (repetition time) and TE = 32 ms (echo time). Since the spin–lattice relaxation rate was only rarely affected by the magnetic particles the increment in phase relaxation rate $1/T$ could be calculated from (*33*)

$$\frac{1}{T} = -\frac{\ln(S/S_0)}{TE}, \qquad [3.24]$$

where S/S_0 denotes the ratio of the signal intensity after and before application of magnetic particles.

According to our model the increment of phase relaxation rate in the presence of magnetic particles in Kupffer cells is given by Eq. [3.19]. For the calculation of relaxation rates one needs to know the radius R_e of the effect volume which itself depends on the induced magnetic dipole moment μ_z around Kupffer cells (Eq. [3.7]). This dipole moment is determined by the amount of intracellular magnetite iron. Since this parameter was not evaluated by Saini *et al.* (*2*) we assumed that for small concentrations of applied magnetic particles the amount of intracellular magnetite iron d is proportional to the applied concentration C,

$$d(C) = K \cdot C, \qquad [3.25]$$

where K is a constant. The dipole moment μ_z is proportional to the amount of intracellular magnetite iron d,

$$\mu_z(d) = \text{const} \cdot d. \qquad [3.26]$$

By means of Eqs. [3.7] and [3.26] one obtains for the sizes of the effect volumes for two different doses of applied magnetite iron C_1 and C_2

$$\frac{R_e(C_1)}{R_e(C_2)} = \left(\frac{C_1}{C_2}\right)^{1/4}. \qquad [3.27]$$

Once the radius R_e for a certain dose C_2 is known, Eq. [3.27] enables one to determine R_e for any dose C_1.

We considered, therefore, the observed increment of the relaxation rate T^{-1} for a certain dose of magnetite iron ($C = 10.9$ μmol Fe/kg body wt). Using Eq. [3.19] and mean intercellular distances $2R_a$ of 40, 60, or 80 μm (*13*), R_e was computed for this concentration. For the determination of the relaxation rate increment as a function of dose, i.e., $T^{-1} = T^{-1}(C)$, we determined first according to Eq. [3.27] $R_e(C)$. The results are shown in Fig. 8. We evaluated then from [3.19] $T^{-1} = T^{-1}(R_e(C))$. This rate is presented in Fig. 9.

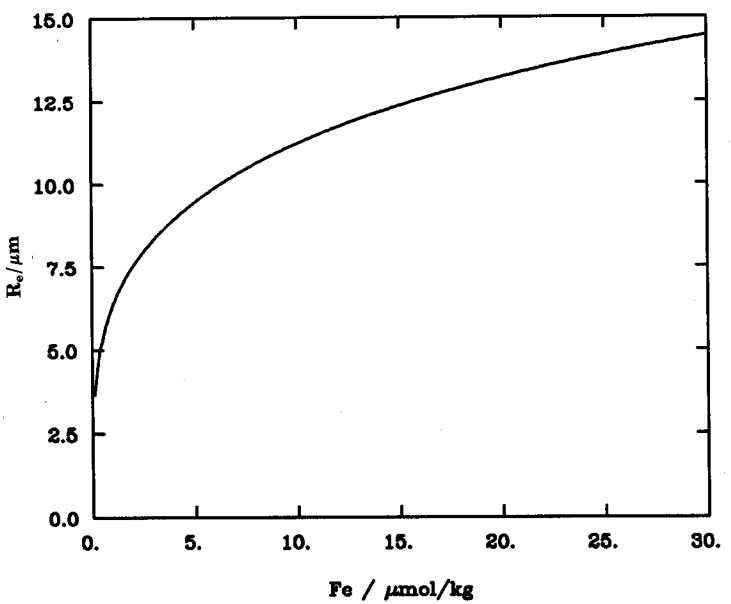

FIG. 8. Dependence of R_e on the dose of magnetite iron. The mean distance of neighboring Kupffer cells ($2R_a$) was assumed to be 40 μm (typical values are actually in the range 50–80 μm). R_e has been evaluated according to Eq. [3.7] assuming a linear relationship between μ_z/G_c and the dose of magnetite iron. Since the proportionality factor between μ_z/G_c and the dose is unknown, we have fitted R_e for a particular iron concentration, namely for 10.9 μmol Fe/kg body wt, for which the relaxation time is known ($T^{-1} = 28.46$ 1/s). The latter had been determined from data by Saini *et al.* (*2*) using Eq. [3.24]. The diffusion coefficient in liver chosen is $D = 1$ μm²/ms.

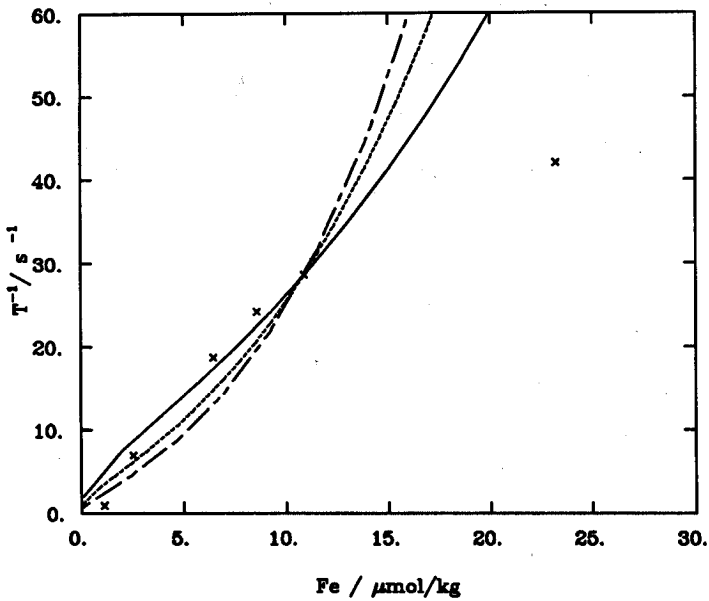

FIG. 9. Dependence of the (incremental) phase relaxation rate T^{-1} on the dose of iron (magnetite). The rate has been evaluated according to Eq. [3.19] using $R_c(c)$ as shown in Fig. 8. Three different mean distances ($2R_a$) of neighboring Kupffer cells are considered: 40 μm (—), 60 μm (-------), and 80 μm (– — – —). The results are compared to relaxation rates (×) obtained from signal intensities of Ref. (*2*) using Eq. [3.24]. (D = 1 $\mu m^2/ms$).

As can be seen from Fig. 9 the best fit of observed and calculated relaxation rates is achieved for an intercellular distance $2R_a$ = 40 μm. The observed relaxation rate for a dose C = 23 μmol Fe/kg body wt is smaller than predicted. In judging this discrepancy one has to keep in mind that the prediction of the relaxation rate has been based on the assumption that the intracellular magnetite concentration is proportional to the applied dose (Eq. [3.25]). Since this pharmacokinetical assumption can be expected to hold only for small doses of magnetite, iron saturation effects on iron uptake by Kupffer cells might explain the above mentioned discrepancy. This explanation actually is confirmed by an observation of Saini *et al.* (*2*) who reported that for a dose of 50 μmol Fe/kg body wt the major part of the intracellular space of Kupffer cells is filled with magnetic particles. This implies that saturation effects occur most likely for doses of about 23 μmol Fe/kg body wt.

3.6. Discussion

In this chapter we have presented a model describing enhanced phase relaxation due to magnetic particles in Kupffer cells. An analytical expression for the relationship between phase relaxation rate enhancement and density of Kupffer cells was obtained for a model which replaces the gradual effect of dipole fields around magnetic Kupffer cells by a discontinuous relaxation rate. As NMR signal intensities depend on phase relaxation rates our result might help to determine, by means of observed contrast

differences, densities of Kupffer cells in liver and, thereby, to detect pathological states of liver tissue.

The most prominent member in the group of liver pathologies is carcinoma which is accompanied by a characteristic reduction in the density of Kupfer cells (*31*). The application of magnetic particles in experimental MRI leads to pronounced contrast enhancement between tumor and normal liver tissue (*31*). The difficulty in conventional diagnosis of liver carcinoma is that the tumor tissue sometimes is highly differentiated, i.e., the tumor tissue exhibits a structure quite similar to that of normal liver tissue (*29*). As a consequence there is only little difference in (i) absorption of X-rays, (ii) reflection of ultrasound waves between tumor and normal liver tissue, and, hence, because of (i) conventional X-ray tomography, and because of (ii) ultrasound reflection may fail in diagnosing liver carcinoma. One successful conventional method left is scintigraphy of liver. The disadvantage of scintigraphy is that scintigrams have a poor spatial resolution, i.e., it is difficult to identify small tumors and to differentiate tumor tissue from normal tissue at the boundary of the tumor. Due to its high spatial resolution MRI does not have such disadvantages.

ACKNOWLEDGMENTS

The authors thank P. Lauterbur for having introduced to them the problems investigated in this article as well as for numerous advice. The work has been supported in part by the National Institutes of Health Grant RR05969.

REFERENCES

1. U. SCHMIEDL, M. OGAN, H. PAAJANEN, M. MAROTTI, L. E. CROOKS, A. C. BRITO, AND R. C. BRASCH, *Radiology* **162,** 205 (1987).
2. S. SAINI, D. D. STARK, P. F. HAHN, J. WITTENBERG, T. J. BRADY, AND J. T. FERRUCCI, *Radiology* **162,** 211 (1987).
3. G. BACIC, M. R. NIESMAN, H. F. BENNET, R. L. MAGIN, AND H. M. SWARTZ, *Magn. Reson. Med.* **6,** 445 (1988).
4. C. TILCOCK, E. UNGER, P. CULLIS, AND P. MACDOUGALL, *Radiology* **171,** 77 (1989).
5. A. VILLRINGER, B. R. ROSEN, J. B. BELLIVEAU, J. L. ACKERMAN, R. B. LAUFFER, R. B. BUXTON, Y. CHAO, V. J. WEDEEN, AND T. J. BRADY, *Magn. Reson. Med.* **6,** 164 (1988).
6. J. MCCONNELL, "The Theory of Nuclear Magnetic Relaxation in Liquids," Cambridge Univ. Press, Cambridge, 1987.
7. P. L. ALTMAN AND P. S. DITTMER, "Respiration and Circulation," Fed. Amer. Soc. Exp. Biol., Bethesda, 1971.
8. O. HARTH, R. F. SCHMIDT, AND G. THEWS, "Physiologie des Menschen" (R. F. Schmidt and G. Thews, Eds.), pp. 558–571, Springer: Berlin/Heidelberg/New York, 1980.
9. D. J. JACKSON, "Classical Electrodynamics," Wiley, New York/London/Sidney, 1966.
10. C. P. SLICHTER, "Principles of Magnetic Resonance," Harper & Row, New York/Evanston/London, 1963.
11. T. CONLON AND R. OETHRED, *Biochim. Biophys. Acta* **288,** 354 (1972).
12. V. V. MORARIU AND G. BENGA, *Biochim. Biophys. Acta* **469,** 301 (1977).
13. SOBOTTA-HAMMERSEN, "Histologie," pp. 110–111 Urban u. Schwarzenberg, München/Wien/Baltimore, 1979.
14. J. GROTE, "Physiologie des Menschen," (R. F. Schmidt and G. Thews, Eds.), pp. 558–571, Springer, Berlin/Heidelberg/New York, 1980.
15. B. ZWEIFACH AND M. INTAGLIETTA, *Microvasc. Res.* **1,** 83 (1968).
16. W. F. LANDIS AND J. R. PAPPENHEIMER, "Handbook of Physiology, Sect. 2," Hamilton, Baltimore, 1963.

differences, densities of Kupffer cells in liver and, thereby, to detect pathological states of liver tissue.

The most prominent member in the group of liver pathologies is carcinoma which is accompanied by a characteristic reduction in the density of Kupfer cells (*31*). The application of magnetic particles in experimental MRI leads to pronounced contrast enhancement between tumor and normal liver tissue (*31*). The difficulty in conventional diagnosis of liver carcinoma is that the tumor tissue sometimes is highly differentiated, i.e., the tumor tissue exhibits a structure quite similar to that of normal liver tissue (*29*). As a consequence there is only little difference in (i) absorption of X-rays, (ii) reflection of ultrasound waves between tumor and normal liver tissue, and, hence, because of (i) conventional X-ray tomography, and because of (ii) ultrasound reflection may fail in diagnosing liver carcinoma. One successful conventional method left is scintigraphy of liver. The disadvantage of scintigraphy is that scintigrams have a poor spatial resolution, i.e., it is difficult to identify small tumors and to differentiate tumor tissue from normal tissue at the boundary of the tumor. Due to its high spatial resolution MRI does not have such disadvantages.

ACKNOWLEDGMENTS

The authors thank P. Lauterbur for having introduced to them the problems investigated in this article as well as for numerous advice. The work has been supported in part by the National Institutes of Health Grant RR05969.

REFERENCES

1. U. SCHMIEDL, M. OGAN, H. PAAJANEN, M. MAROTTI, L. E. CROOKS, A. C. BRITO, AND R. C. BRASCH, *Radiology* **162,** 205 (1987).
2. S. SAINI, D. D. STARK, P. F. HAHN, J. WITTENBERG, T. J. BRADY, AND J. T. FERRUCCI, *Radiology* **162,** 211 (1987).
3. G. BACIC, M. R. NIESMAN, H. F. BENNET, R. L. MAGIN, AND H. M. SWARTZ, *Magn. Reson. Med.* **6,** 445 (1988).
4. C. TILCOCK, E. UNGER, P. CULLIS, AND P. MACDOUGALL, *Radiology* **171,** 77 (1989).
5. A. VILLRINGER, B. R. ROSEN, J. B. BELLIVEAU, J. L. ACKERMAN, R. B. LAUFFER, R. B. BUXTON, Y. CHAO, V. J. WEDEEN, AND T. J. BRADY, *Magn. Reson. Med.* **6,** 164 (1988).
6. J. MCCONNELL, "The Theory of Nuclear Magnetic Relaxation in Liquids," Cambridge Univ. Press, Cambridge, 1987.
7. P. L. ALTMAN AND P. S. DITTMER, "Respiration and Circulation," Fed. Amer. Soc. Exp. Biol., Bethesda, 1971.
8. O. HARTH, R. F. SCHMIDT, AND G. THEWS, "Physiologie des Menschen" (R. F. Schmidt and G. Thews, Eds.), pp. 558–571, Springer: Berlin/Heidelberg/New York, 1980.
9. D. J. JACKSON, "Classical Electrodynamics," Wiley, New York/London/Sidney, 1966.
10. C. P. SLICHTER, "Principles of Magnetic Resonance," Harper & Row, New York/Evanston/London, 1963.
11. T. CONLON AND R. OETHRED, *Biochim. Biophys. Acta* **288,** 354 (1972).
12. V. V. MORARIU AND G. BENGA, *Biochim. Biophys. Acta* **469,** 301 (1977).
13. SOBOTTA-HAMMERSEN, "Histologie," pp. 110–111 Urban u. Schwarzenberg, München/Wien/Baltimore, 1979.
14. J. GROTE, "Physiologie des Menschen," (R. F. Schmidt and G. Thews, Eds.), pp. 558–571, Springer, Berlin/Heidelberg/New York, 1980.
15. B. ZWEIFACH AND M. INTAGLIETTA, *Microvasc. Res.* **1,** 83 (1968).
16. W. F. LANDIS AND J. R. PAPPENHEIMER, "Handbook of Physiology, Sect. 2," Hamilton, Baltimore, 1963.

17. D. BARSKY, B. PÜTZ, K. SCHULTEN, AND R. L. MAGIN, *Magn. Reson. Med.* **24,** 1 (1992).
18. P. A. BOTTOMLEY, C. J. HARDY, R. E. ARGERSINGER, AND G. ALLEN-MOORE, *Med. Phys.* **14,** 1 (1987).
19. H. KNOCHE, "Lehrbuch der Histologie," pp. 183–186, Springer, Berlin/Heidelberg/New York, 1979.
20. P. GILLIS AND S. H. KOENIG, *Magn. Reson. Med.* **5,** 323 (1987).
21. H. C. TORREY, *Phys. Rev.* **104,** 563 (1956).
22. W. NADLER AND K. SCHULTEN, *J. Chem. Phys.* **82,** 151 (1985).
23. W. H. PRESS, B. P. FLANNERY, S. A. TEUKOLSKY, AND W. T. VETTERLING, "Numerical Recipes," Cambridge Univ. Press, Cambridge, 1986.
24. E. GRUNDMANN, "Einführung in die allgemeine Pathologie," p. 159, Fischer, Stuttgart/New York, 1981.
25. L. HENQUELL, C. L. ODOROFF, AND C. R. HONIG, *Circ. Res.* **41,** 400 (1977).
26. P. ANVERSA, C. BEGHI, Y. KIKKAWA, AND G. OLIVETTI, *Circ. Res.* **58,** 26 (1986).
27. J. T. ROBERTS AND J. T. WEARN, *Am. Heart J.* **21,** 617 (1941).
28. H. R. FIGULLA, F. VETTERLEIN, V. WIEGAND, S. SCHÜLER, AND H. KREUZER, *Zeitsch. Kardiol.* **76**(Suppl. 3), 152 (1987).
29. W. SANDRITTER AND C. THOMAS, "Histopathologie," p. 165, Schattauer, Stuttgart/New York.
30. W. BERGER, F. A. GRIES, TH. KOSCHINSKY, M. TOELLER, AND G. STROHMEYER, (W. Siegenthaler, W. Kaufmann, H. Hornbostel, and H. D. Waller, Eds.), pp. 15.1–15.72, "Lehrbuch der inneren Medizin," Georg Thiemes, Stuttgart/New York, 1984.
31. S. SAINI, D. D. STARK, P. F. HAHN, J. C. BOUSQUET, J. INTROCASSO, J. WITTENBERG, T. J. BRADY, AND J. T. FERRUCCI, *Radiology* **162,** 217 (1987).
32. C. KITTEL, "Einführung in die Festkörperphysik," Oldenbourg, München/Wien, 1980.
33. R. C. BRASCH, G. E. WESBEY, C. A. GOODING, AND M. A. KOERPER, *Radiology* **150,** 767 (1984).